IEEE Access
Multidisciplinary | Rapid Review | Open Access Journal

Received November 29, 2017, accepted January 10, 2018, date of publication January 15, 2018, date of current version March 9, 2018.

Digital Object Identifier 10.1109/ACCESS.2018.2793299

Channel Characterization of Acoustic Waveguides Consisting of Straight Gas and Water Pipelines

LIWEN JING, (Student Member, IEEE), ZHAO LI, (Member, IEEE), YUE LI, (Student Member, IEEE), AND ROSS D. MURCH, (Fellow, IEEE)
Department of Electronic and Computer Engineering, The Hong Kong University of Science and Technology, Hong Kong

Corresponding author: Zhao Li (eelizhao@ust.hk)

This work was supported by the Hong Kong Research Grants Council through the General Research Fund under Grant 16210415 and the Theme-based Research Scheme under Grant T21-602/15R.

ABSTRACT Characterizing acoustic waveguide channels is becoming important for the development of communication and signal processing applications across diverse fields ranging from urban water supply systems to oil and gas distribution pipeline networks. These applications include sonar and transmission systems in support of leak detection, blockage location, sensing, monitoring, and signaling for example. In this paper, we provide experimental results and models for the wideband channel characterization of acoustic waveguides formed from gas and water pipelines over the 1–50 kHz frequency band. Experimental results are provided for two straight pipe systems comprising an acrylic pipe filled with air and a steel pipe filled with water. A mode-based analytical model for predicting acoustic wave propagation in rigid and elastic pipes is proposed with deterministic and stochastic characteristics both considered. Good matching is demonstrated between the model predictions and experimental results in terms of dispersion curves, channel spectrograms, and delay spread. A key finding is that acoustic waveguides filled with water should be treated as elastic pipes, and they have significantly different characteristics from those filled with gas, which can usually be treated as rigid pipes. Furthermore for the steel-water waveguide pipeline, link budget calculations and noise power spectral density measurements reveal that a communication range of more than 50 m can be obtained.

INDEX TERMS Channel characterization, acoustic waveguide, cylindrical pipe channel, channel modeling, propagation modes, normal mode, delay-spread, noise.

I. INTRODUCTION

Channel characterization is a critical building block in the design and development of communication and signal processing systems and these have many important industrial, government and consumer applications. Channel characterization for ocean acoustic, wireless, wired, and optical channels has a long history and numerous results and models have been reported and developed [1]–[6]. Another channel that is becoming increasingly important is that formed by acoustic waveguide channels consisting of urban water supply systems (UWSS), oil and gas distribution pipeline networks [7]–[9]. These systems support the lives of billions of people and therefore their safe and reliable operation is critical. For example contamination or interference with UWSS can have serious health and security implications, while pipe failures can disrupt lives, businesses and cause damaging flooding. However current methods for sensing, collecting and processing data in pipeline networks to address these issues are inadequate. One possible approach to acquiring pipeline data is through the development of acoustic communication and sonar systems that operate inside pipelines in support of sensor networks, robotic inspection and robotic navigation [10], [11]. The reason for this is that traditional wireless magneto-inductive [12] and RF communication techniques are not always applicable in the pipeline environment which can feature metal pipes buried deep in the ground for example. Motivated by this background, channel characterization for acoustic waveguides consisting of pipelines is considered in this paper.

In related work on acoustic channels there has been a focus on wireless acoustic communication in deep and shallow open water columns in oceans, rivers and lakes [1], [13], [14]. Distinctive features of the acoustic channel in oceans include wave reflection from the ocean surface and refraction resulting from spatial variability of sound speed, both causing extensive time-varying multipath [13], [15]. In addition

there exist high levels of non-Gaussian ambient noise from snapping shrimp in warmer water, ice cracking in polar regions, breaking waves, rain and distant shipping. Furthermore strong Doppler effects are present due to the motion of the mobile stations.

In related work on waveguide channels, fiber-optic communication is the most developed data transmission system utilizing waveguides [16]. Channel characterization of waveguides is also related to previous work on wireless communication in tunnels because the structure of the tunnel forms a waveguide for electromagnetic waves. [17], [18]. Results for communication in acoustic waveguides is much more limited. According to the existing physical models for acoustic vibrations in waveguides [19], [20], both wave speed and wave propagation paths are sensitive to pipe material and the material surrounding the pipe, which form the boundaries of the waveguide. In addition, the effect of mode cutoffs becomes significant due to the wideband nature of the acoustic signals and the relatively small pipe diameter compared to the wavelengths considered. This dimension difference also generates different spatial-dependent channel characteristics under mobile conditions, such as when robots are traveling inside the pipeline. Further investigation of channel characterization for acoustic waveguide channels is therefore required and is a building block for designing communication systems and sonar based methods for finding defects and monitoring pipelines. While our motivation is primarily related to UWSS, applications extend well beyond that and include air, gas and oil pipelines which also exhibit similar characteristics.

In this work we describe our measurements and propose models for acoustic waveguides channels consisting of straight pipelines filled with gas or water. To our knowledge only very limited experimental results have been provided for characterizing acoustic waveguide channels previously. The following new contributions are made in this paper: (a) we provide systematic experimental results for channel characterization of steel-water and acrylic-air pipelines; (b) we propose a general acoustic waveguide channel model for both rigid and elastic cylindrical pipes that is compared and verified with our experimental channel measurements; (c) we determine typical communication channel parameters such as link budget, channel capacity, coherence bandwidth, path loss and fading; and (d) determine the dispersion characteristics of the acoustic waveguides and demonstrate their effects by using transfer functions, impulse response, spectrogram and dispersion curves. Through these findings it is also demonstrated that waveguides with a liquid media such as water must take into account the elasticity of the pipe material even for seemingly rigid pipelines such as steel and that channel characteristics change significantly across mode cutoff frequencies.

This paper is organized as follows: in section II, a general deterministic model of wave propagation in cylindrical waveguides is provided, in which both rigid and elastic boundary conditions are taken into consideration. We also derive dispersion curves (space-frequency representation) and spectrograms (time-frequency representation) from the modeled transfer function. Stochastic effects such as receiver movement are also considered to arrive at statistical definitions of key channel characteristics. In section III, measurement results in acrylic-air and steel-water channels are presented and compared with model predictions. These results are used to validate the model across a wide range of parameters. In addition we provide an estimation of the noise power spectral density in the steel-water waveguide so that we can determine link budget, capacity and communication range. Finally conclusions and potential directions for future research are provided in section IV.

To avoid confusion we also define some notation. For a quantity, x expressed in dB we use the form x [dB] to distinguish it from its linear form which is written as x. We also use the assumed time harmonic variation $e^{-j2\pi ft}$.

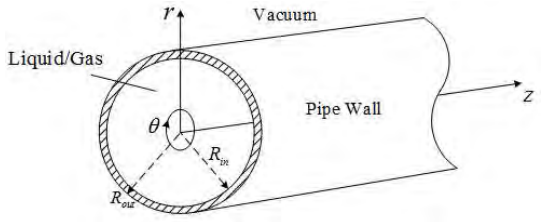

FIGURE 1. Acoustic waveguide shown in cylindrical coordinates.

II. ACOUSTIC CHANNEL MODELING IN CYLINDRICAL WAVEGUIDE

The acoustic waveguide channel considered consists of an inner liquid/gas medium, a solid cylindrical waveguide (pipe wall) and an outer vacuum space as shown in Fig. 1. Cylindrical coordinates (r, θ, z) are utilized with the z-axis defined along the cylindrical axis and where R_{in} and R_{out} are the inner and outer radius of the waveguide pipe wall as also shown in Fig. 1. The channel characterization problem is then defined as determining the output received voltage $V_{out}(f, r, \theta, z)$ from a hydrophone or microphone located at (r, θ, z) due to an input transmit voltage $V_{in}(f, r, \theta, z)$ applied to a projector or speaker at location $(a, 0, 0)$ where $a \leq R_{in}$ for each frequency f. The resulting transfer function or relation between $V_{out}(f, r, \theta, z)$ and $V_{in}(f, a, 0, 0)$ can be obtained by utilizing the classical separable expression for the acoustic pressure inside a cylindrical waveguide. This is found in terms of modes using Bessel and Exponential functions [20], [21] and by incorporating the transducer characteristics relating received and transmitted voltages to acoustic pressures [22]. Using this approach we write the channel transfer function in general form as,

$$\begin{aligned} H(f, r, \theta, z) &= \frac{V_{out}(f, r, \theta, z)}{V_{in}(f, a, 0, 0)} \\ &= B(f) \sum_{n=0}^{\infty} \sum_{m=0}^{\infty} A_{nm}(f) J_{nm}(r) \cos(n\theta) \\ &\quad \times e^{jk_{nm}(f)z} e^{-\alpha_{nm}(f)z}, \end{aligned} \tag{1}$$

TABLE 1. Modeled cutoff frequencies of two acoustic waveguide channels (Channel 1 is acrylic pipe filled with air of 5 cm inner diameter; Channel 2 is steep pipe filled with water of 6.5 cm inner diameter).

	(0,0)	(0,1)	(0,2)	(0,3)	(1,0)	(1,1)	(1,2)	(1,3)	(2,0)	(2,1)	(2,2)	(2,3)
Channel 1 (kHz)	0.0	8.3	15.2	22.0	4.0	11.5	18.5	25.3	6.6	14.5	21.6	28.5
Channel 2 (kHz)	0.0	0.0	22.1	32.1	13.6	14.6	34.1	43.1	18.6	25.6	28.6	46.6

where the integer pair (n, m) denotes a particular mode in which angular variation is related to the integer n and can be written in terms of $\cos(n\theta)$ (because without loss of generality the transmitter is located at $\theta = 0$) and radial variation is described by the function $J_{nm}(r)$ consisting of combinations of Bessel functions [20], [21] and related to both mode indices (n, m). The function $A_{nm}(f)$ denotes the amplitude of mode (n, m), while $k_{nm}(f)$ represents the real wave number of the channel and $\alpha_{nm}(f)$ characterizes the frequency dependent exponential attenuation of the mode. Finally the characteristics of the receiver and transmitter transducers that relate voltages to pressures are captured by $B(f)$ [22]. It should also be noted that channel variation such as fading occurs when the receiver or transmitter is moving, such as in robotic based pipe inspection, so that z becomes a function of time and these stochastic effects will be discussed later in the section.

A special configuration of (1) occurs when the transmitter is located at the origin $r = 0$ where the system becomes circularly symmetric so that $n = 0$ and the double sum in (1) becomes a single sum.

A. DISPERSION CURVES

One key parameter in the propagation of the modes is the wavenumber $k_{nm}(f)$ and the relationship between $k_{nm}(f)$ and f is usually shown by a $f - k_{nm}(f)$ dispersion curve. The wavenumber is only greater than 0 above a certain cutoff frequency f_{nm} and with this characteristic it can be deduced that a particular mode only propagates when its frequency f is above cut-off $f > f_{nm}$. The existence of the cutoff frequency and corresponding wavenumber $k_{nm}(f)$ at a certain frequency is determined by the boundary conditions between the inner medium and waveguide wall material. When the waveguide shown in Fig. 1 is filled with gas, because of the significant difference in acoustic impedance (defined by the product of medium density and the wave speed), the acoustic field coupled in the waveguide wall is very weak so that the inner pipe wall ($r = R_{in}$) can be treated as a rigid boundary and the modes and their amplitudes can be found straightforwardly as described in [20] and [21]. In particular the cutoff frequency f_{nm} and wavenumber k_{nm} can be calculated from the roots of the derivative of Bessel functions of the first kind order n so that the wavenumber can be written as $k_{nm}(f) = \frac{2\pi}{c}\sqrt{f^2 - f_{nm}^2}$ [20], [21]. As a specific example for a rigid pipe of 5 cm diameter filled with air the dispersion curves are plotted in Fig. 2(a) and cutoff frequencies are listed in Table 1 row 1. Unlike metallic waveguides in electromagnetics there is one mode with zero cutoff and it travels in the form of a planar wave with no variation in either the radial or angular coordinates. In addition for this example it can be seen from Table 1 up to 8 main modes ($m \leq 3, n \leq 2$) have cutoffs within 20 kHz and only four of these exist if the mode configuration is circularly symmetric ($n = 0$).

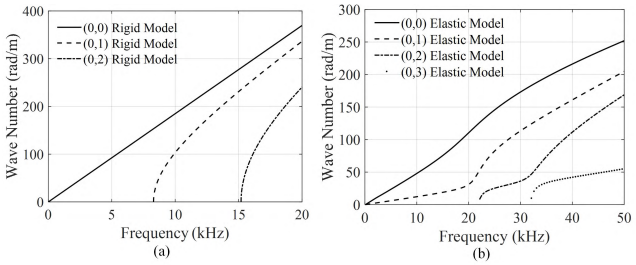

FIGURE 2. Modeled dispersion curves for both rigid and elastic boundaries when $n = 0$ (a) acrylic-air waveguide channel, (b) steel-water waveguide channel.

For the situation where the inner medium of the waveguide is liquid, the acoustic wave propagates in both the inner medium and waveguide pipe wall, which provides more complicated elastic boundary conditions and these are detailed in Appendix. Even for seemingly rigid pipes such as steel the elasticity of the waveguide wall must still be taken into account and the wall cannot be taken as rigid for media such as water. As a specific example for a steel pipe of 6.5 cm diameter filled with water the dispersion curves and cutoffs are given in Fig. 2(b) and Table 1 row 2 respectively. Differences from the rigid pipe case are significant and include two modes with zero cutoff and 12 main modes within 50 kHz. Only four of these exist if the mode configuration is circularly symmetric ($n = 0$). A hallmark of the elastic pipe is that no straightforward relation between the wavenumber $k_{nm}(f)$ and frequency can be written and it must be found numerically as detailed in Appendix.

In reality, the dispersion curves cannot always be obtained through a physical model due to the uncertainty of material and geometry properties of the pipe and instead, the transfer function will need to be obtained experimentally. To make a connection between transfer function and dispersion curves, we first merge terms together in (1) so that $G_{nm}(f, r, \theta, z) = B(f)A_{nm}(f)J_{nm}(r)\cos(n\theta)e^{-\alpha_{nm}(f)z}$, simplifying (1) to

$$H(f, r, \theta, z) = \sum_{n=0}^{\infty}\sum_{m=0}^{\infty} G_{nm}(f, r, \theta, z)e^{jk_{nm}(f)z}. \qquad (2)$$

The dispersion curve can then be found by applying the spatial domain Fourier transform to (2) with respect to the

$z-$coordinate as

$$\mathscr{H}(f, r, \theta, k) = \sum_{n=0}^{\infty}\sum_{m=0}^{\infty}\mathscr{G}_{nm}(f, r, \theta, k) \otimes \delta(k - k_{nm}(f)), \tag{3}$$

where $\otimes$ denotes convolution, $\delta(\cdot)$ denotes the Dirac delta function and $\mathscr{G}_{nm}(\cdot)$ is the Fourier transformation pair of $G_{nm}(\cdot)$ in the spatial wavenumber domain. It is shown in (3) that the energy is mainly constrained along the mode wavenumber $k_{nm}(f)$, which implies the dispersion curve can be observed as a "bright curve" in the frequency-wavenumber domain. For the two pipe examples described here their measured dispersion curves are shown in the experimental results described in section III. Thus, those curves provide methods to distinguish different modes in the channel for different media and pipe materials.

B. SPECTROGRAMS

The dispersion curves can only be obtained by measuring the transfer function H along the z-axis and performing a subsequent Fourier transform. In practice these measurements can be tedious or even impossible and therefore we also introduce the time-frequency spectrogram [23] as a method for indirectly showing the dispersion relationship. This is obtained by expanding the wavenumber as a Taylor series with respect to f at a center frequency f_0 so that $k_{nm}(f)$ can be written as

$$k_{nm}(f) = k_{nm}(f_0) + \frac{dk_{nm}}{df}|_{f_0}(f - f_0) + \frac{1}{2}\frac{d^2k_{nm}}{df^2}|_{f_0}(f - f_0)^2 + \cdots. \tag{4}$$

The terms in (4) are also related to group velocity v_{nm} and group velocity dispersion (GVD) D_{nm}, written as

$$v_{nm}(f_0) = \frac{2\pi df}{dk_{nm}}|_{f_0}, \tag{5}$$

$$D_{nm}(f_0) = \frac{1}{4\pi^2}\frac{dk_{nm}^2}{d^2f}|_{f_0}. \tag{6}$$

For mode (n, m), v_{nm} determines the signal arrival time, and D_{nm} is the amount of dispersion or pulse spreading in that mode. The dispersion or time expansion of a pulse within a mode can then be written as $\Delta\tau = zD2\pi(f - f_0)$. In addition the excess delay at f_0 across all modes can be written as $z(v^{\max}(f_0)^{-1} - v^{\min}(f_0)^{-1})$ where $v^{\max}$ and $v^{\min}$ are the maximum and minimum group velocity across all of the propagating modes respectively.

Within a narrow frequency band we can approximate the Taylor series by its first two terms and the maximum bandwidth Δf for which the first two terms of (4) are a good approximation. This bandwidth can be written as

$$\Delta f < \frac{1}{\pi v_{nm}D_{nm}}, \tag{7}$$

and can be considered the bandwidth over which pulse spreading does not occur significantly. The approximate wavenumber expression of (4) is then written as

$$k_{nm}(f) = k_{nm}(f_0) + \frac{2\pi(f - f_0)}{v_{nm}(f_0)} = \left[k_{nm}(f_0) - \frac{2\pi f_0}{v_{nm}(f_0)}\right] + \frac{2\pi f}{v_{nm}(f_0)}. \tag{8}$$

By substituting (8) into (2) and merging the f_0 related terms with the amplitude term, we have a narrow band transfer function

$$\widetilde{H}(f, f_0, r, \theta, z) = \sum_{n=0}^{\infty}\sum_{m=0}^{\infty}G_{nm}(f, r, \theta, z) \cdot e^{j\frac{2\pi f}{v_{nm}(f_0)}z} \cdot W\left(\frac{f - f_0}{\Delta f}\right). \tag{9}$$

$W(f)$ is an appropriate window function (such as a raised cosine) with unit bandwidth so that the bandwidth Δf specifies the bandwidth over which the narrowband model remains accurate and can be estimated from (7). Taking the inverse Fourier transform with respect to f and noticing the term $z/v_{nm}(f_0)$ represents the arriving time τ_{nm}, we can obtain a narrow-band impulse response

$$\begin{aligned}\tilde{h}(\tau, f_0, r, \theta, z) &= \sum_{n=0}^{\infty}\sum_{m=0}^{\infty}g_{nm}(\tau, r, \theta, z) \otimes w(\tau\Delta f) \times e^{j2\pi f_0\tau}\Delta f \otimes \delta(\tau - \tau_{nm}(f_0)) \\ &= e^{j2\pi f_0\tau}\Delta f\sum_{n=0}^{\infty}\sum_{m=0}^{\infty}g_{nm}(\tau, r, \theta, z) \otimes w((\tau - \tau_{nm}(f_0))\Delta f),\end{aligned} \tag{10}$$

where τ is used to represent delay time, $g_{nm}(\tau, r, \theta, z)$ and $w(\tau)$ are the inverse Fourier transforms of $G_{nm}(f, r, \theta, z)$ and window $W(f)$ respectively. (10) indicates that multiple modes of propagating waves arrive at a receiver with separate paths carrying the same symbol sequences with different arrival times. The bandwidth of the window Δf limits the time resolution of the paths to be approximately $1/\Delta f$.

If we scan the center frequency across a band so that the center frequency is defined as $f_p = f_s + p\delta f$ where f_s is the start of the band and δf (usually with $\delta f < \Delta f$) is taken as the step or sample frequency with $(p = 0, 1, 2, \cdots (P - 1))$ we can write the resulting narrowband impulse response at f_p over bandwidth Δf as $\tilde{h}(\tau, f_p, r, \theta, z)$. We can then form the spectrogram $\mathbb{H}(\tau, p)$ where

$$\mathbb{H}(\tau, p) = \tilde{h}(\tau, f_p, r, \theta, z). \tag{11}$$

The spectrogram can be thought of as a two dimensional image where each row is the narrowband impulse response at frequency f_p. This also implies that there will be "bright curves" in the frequency-time domain. For the two examples described already their spectrograms as predicted by the model (1) are shown in figure 3. Thus, these curves can also be used to distinguish different modes in the channel by taking a single measurement at one point z instead of multiple positions as for (3). This allows a significant reduction in the measurement setup requirement.

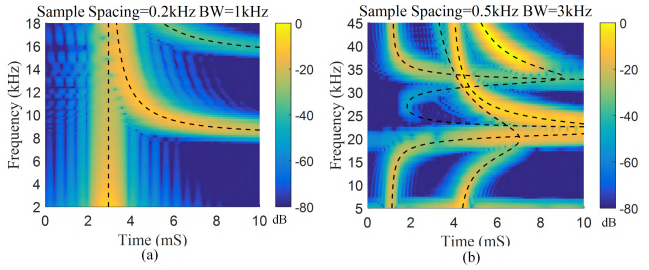

FIGURE 3. Modeled channel spectrograms where the overlaid dashed lines are the ridges of the "bright curves" and found from the predicted group delay (a) acrylic-air channel at 1 m, (b) steel-water channel at 5.8 m.

The spectrogram (11) is related to the dispersion curve by noting that at a fixed position z each "bright curve" is a measure of the group delay for that mode. Since group delay is related to the wavenumber through (5) we can use integration to obtain an expression for $k_{nm}(f)$ as

$$k_{nm}(f) = 2\pi \int_0^f \frac{1}{\nu_{nm}} df + k_{nm}(0), \tag{12}$$

where $k_{nm}(0)$ is the constant of integration and can be taken as the wavenumber at $f = 0$. In essence we can straightforwardly use each "bright curve" of the spectrogram as an estimate of the group velocity for that mode and integrate with respect to frequency. Since most modes have $k_{nm} = 0$ at $f = 0$ we can usually take the arbitrary constant as zero. For those few modes (typically one mode only) for which the wavenumber is not zero at $f = 0$ (as for elastic pipes) we need to estimate the arbitrary constant in order to determine $k_{nm}(0)$ using the model (1).

C. MODE AMPLITUDES AND PROPAGATION LOSS

The mode amplitude $A_{nm}(f)$ is also an important parameter in the model. In principle, $A_{nm}(f)$ can be obtained through expanding the source into an orthogonal Fourier-Bessel series for a point source or a transducer source in both rigid and elastic pipes, but it is often easier to obtain the amplitudes directly from the measurements as discussed in the next section. The attenuation of the modes $\alpha_{nm}(f)$ allows the inclusion of distance dependent loss into the model and this loss arises from both leakage and loss mechanisms in the wall. Distance dependent loss typically depends on $(f - f_{nm})$ where f_{nm} is the cutoff frequency of mode (n, m). This dependence trend can be deduced from the interpretation of modes as rays [24] and noting that the rays propagate along the pipeline by reflecting off the pipe walls. Propagation loss in this viewpoint then primarily occurs from the wall reflections. Therefore as the operating frequency increases away from cutoff the number of reflections per unit distance decreases, leading to decreases in loss. In the measurement result section next we provide estimates of propagation loss $\alpha_{mn}(f)$.

D. IMPULSE RESPONSE

The wideband channel response can be obtained from the inverse Fourier transform of (2) but that does not provide intuition about its form. Insight into the wideband channel can be obtained by considering that the group delay and dispersion for each mode is a function of frequency and therefore the path delay for each mode and its width changes with frequency. An approximate wideband model can be formed by considering the addition of all the narrowband impulse response functions in (11) or equivalently projecting the spectrogram onto the time axis (with $\delta f = \Delta f$). We then arrive at the expression

$$\begin{aligned} h(\tau, r, \theta, z) &= \sum_{p=0}^{P-1} \tilde{h}_p(\tau, f_p, r, \theta, z) \\ &= \Delta f \sum_{p=}^{P-1} \sum_{n=0}^{\infty} \sum_{m=0}^{\infty} g_{nm}(\tau, r, \theta, z) \\ &\quad \otimes w((\tau - \tau_{nm}(f_p))\Delta f) e^{j2\pi f_p \tau}, \end{aligned} \tag{13}$$

which incorporates the effect of dispersion within a mode through the p index so that at each frequency f_p the group velocity is in general different so the signal has different delays. This expression may be written in a more compact form [25]

$$h(\tau, r, \theta, z) = \sum_{k=0}^{K} a_k(\tau, r, \theta, z) w((\tau - \tau_k)\Delta f), \tag{14}$$

where the total number of multipath K is taken as the largest delay divided by the time resolution $\lceil z\Delta f / \nu^{\max} \rceil$ and paths in the same delay bin τ_k (bin size of $1/\Delta f$) are lumped together to form the complex amplitude $a_k(t)$ and is a sum over terms with the same delay. The expression (13) is approximate because the resolution of the wideband response is limited to that of the window function w. For an exact high resolution form it is necessary to take the inverse Fourier transform of (2).

E. STOCHASTIC CHARACTERIZATION

If devices such as mobile robots are used to inspect the inside of the pipe for defects, the receiver or transmitter will be moving, and therefore random variations in the channel characteristics will occur so that the channel becomes a stochastic process. This is most easily observed by considering movement along the z-axis of the waveguide so that destructive and constructive inference of the different modes (14) will occur leading to fading and Doppler. The channel is not however wide sense stationary (WSS) as channel parameters such as excess delay vary with z (and therefore movement over time t) and it also does not exhibit uncorrelated scattering (US) since the channel delay taps are functions of frequency. However over short time intervals Δt and small bandwidths Δf we can consider the channel to be WSSUS. Careful application of ensemble averages must therefore be used to estimate channel parameters such as power delay profile and delay spread. The power delay profile or multipath intensity profile [26], [27] is defined as

$$A(\tau) = \mathcal{E}\{\tilde{h}(\tau, f_0, r, \theta, z)\tilde{h}^*(\tau, f_0, r, \theta, z)\}, \tag{15}$$

where $\mathcal{E}$ denotes the ensemble expectation of the narrowband impulse response $\tilde{h}(\tau, f_0, r, \theta, z)$ and f_0 is the center frequency of the narrowband Δf. Assuming the process is pseudo-stationary over time Δt and that it is also ergodic (15) can be written as [27]

$$A(\tau) = \frac{1}{\Delta T} \int_{-\Delta T/2}^{\Delta T/2} \tilde{h}(\tau, f_0, r, \theta, z) \tilde{h}^*(\tau, f_0, r, \theta, z) d\tau. \tag{16}$$

We can then estimate the mean excess delay and root mean square (RMS) delay spread by equation (17) and (18)

$$\overline{\tau} = \frac{\int_0^\infty \tau A(\tau) d\tau}{\int_0^\infty A(\tau) d\tau}, \tag{17}$$

$$\tau_{rms} = \sqrt{\frac{\int_0^\infty (\tau - \overline{\tau})^2 A(\tau) d\tau}{\int_0^\infty A(\tau) d\tau}}. \tag{18}$$

III. MEASUREMENT RESULTS

Measurements of the channel characteristics for two types of acoustic waveguide channels have been obtained and are compared with our proposed model. Measurement and model predictions of transfer functions, dispersion curves, spectrograms, impulse responses, delay spread, power delay profile, fading, noise power spectral density, capacity and link budget are presented.

The first type of acoustic waveguide we consider is the rigid pipe scenario and consists of a straight acrylic pipe with 5 cm diameter, 1.2 m length and filled with air (to simulate gas). The pipe is open at both ends as shown in Fig. 4. A magnetic speaker (DB Unlimited model SM400608-1) and an electric condenser microphone (Azden model SMX-10) are mounted at the center of the pipe as the transmitter and receiver. Due to the center positioning of the transducers we expect the $n = 0$ modes to be dominant. The microphone has flat RVS (Receive Voltage Sensitivity) at audio frequency range and the sensitivity is -160 dB re 1 V/μPa at 1 kHz. The speaker TVR (Transmit Voltage Response) follows a general magnetic speaker frequency response with two peaks at 4 kHz and 10 kHz and it has a TVR of 53.7 dB re 1 μPa/V at 1 m at 1 kHz. The distance is measured between the acoustic centers of the speaker and microphone. Measurements are taken at 100 evenly spaced locations along the pipe from 0.1 m to 1.1 m ($z = [0.1, 1]$) with 1 cm intervals. This acoustic waveguide has the same diameter and material as the rigid pipe example in section (II). Therefore the cut-off frequencies shown in the first row of Table 1 as well as the dispersion curves in Fig. 2a and spectrogram in Fig. 3a can be used for the model predictions. The speed of propagation in air is taken as 340 m/s so that the wavelength varies between 0.17 m and 0.017 m for the frequency range 2-20 kHz.

The second type of acoustic waveguide we consider is the water pipe and consists of a straight pipe constructed from steel (5.8 m length and 6.5 cm diameter) filled with static tap water. The pipe is terminated with water tanks at each end and is slightly tilted to remove air bubbles as shown in Fig. 4.

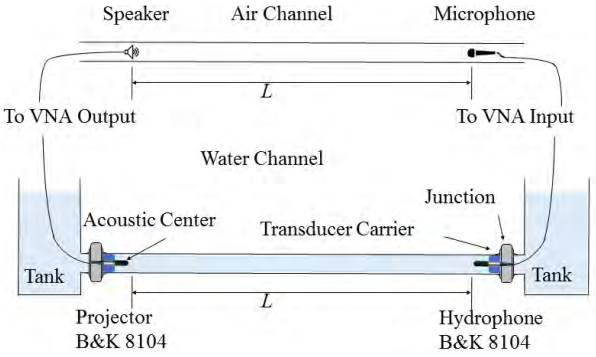

FIGURE 4. Experimental setup for the acrylic-air and steel-water pipelines.

Two piezoelectric transducers (Brüel & Kjær model 8104) are mounted at the center of the water pipe at each end and configured as a projector and hydrophone respectively. Due to the center positioning of the transducers we expect the $n = 0$ modes to be dominant. When configured as a hydrophone the frequency response of the 8104 transducer is flat (within +/−3 dB) from 0-200 kHz and it has a RVS of −206 dB re 1 V/μPa. When configured as a projector the frequency response of the 8104 transducer has the typical k^4 (40 dB/decade) [22] dependence until its resonance peak which occurs at around 200 kHz and it has a TVR of 109 dB re 1 μPa/V at 1 m at 15 kHz. The projector is fixed at 2 m from one end of the pipe (defined as $z = 0$) and the hydrophone is moved from 0.9 m to 2.9 m ($z = [0.9, 2.9]$) at 1 cm intervals to provide 200 evenly spaced measurement locations along the cylinder axis of the pipe. The transducers are mounted at the center of the pipe by 3D printed plastic carriers. The carriers are moved by attaching a magnet along them, so that we can control the location of the transmitters and receivers inside the pipe by moving a magnet from the outer surface of the pipe. The distance is measured between the acoustic centers of the two transducers and the transducer feeding cables are kept taut behind the transducers so they do not interfere with the measurements. This acoustic waveguide has the same diameter and material as the elastic pipe example in the previous section and therefore the predicted cutoff frequencies shown in the second row of Table 1 as well as the dispersion curves in Fig. 2b and spectrogram in Fig. 3b can be used for the model predictions. The speed of propagation in water is taken as 1480 m/s so that the wavelength varies between 0.296 m and 0.0296 m for the frequency range 5-50 kHz.

A vector network analyzer (VNA) Omicron Bode 100 allows the acquisition of the channel frequency response between the transducers. From this we can obtain time domain responses. The VNA has built-in tunable transceivers that can automatically sweep through a wide frequency band from 1 Hz to beyond 50 kHz and acquires the channel frequency response with both amplitude and phase information at all selected frequency points. In our measurements we

use a sampling bandwidth of 10 Hz or 100 Hz depending on the results required. Hence we obtain between 451 and 4501 frequency samples across the 5-50 kHz band in steel-water channel, and between 181 and 1801 frequency samples across the 2-20 kHz band in acrylic-air channel. For the water pipe waveguide a power amplifier (Brüel & Kjær model 2713) is connected before the transmitter to provide up +/−100 V output voltage and the VNA is calibrated so that the effects of the power amplifier are removed. The VNA sensitivity is limited by its internal noise and given that there is also a maximum transmit output the maximum path loss that can be measured is around 150 dB. In this work we define path loss as

$$PL(f)[dB] = V_{tr}(f)[dBV] - V_{re}(f)[dBV], \tag{19}$$

where V_{tr} and V_{re} are the signal voltages at the terminals of the projector/speaker and hydrophone/microphone respectively (dBV is defined as $20 \log V/1V$). For acoustic systems using piezoelectric transducers the output and input are usually specified as voltages because the transducers have a large reactance [22]. With this definition the $PL(f)$ can be directly obtained from the VNA measurements and includes the characteristics of both the channel and transducers.

The effect of the transducers can be de-embedded from $PL(f)$ by removing the transducer characteristics and more specifically the de-embedded path loss is defined here as

$$PL_{deembed}(f)[dB] = V_{tr}(f)[dBV] - V_{re}(f)[dBV] - B(f)[dB]. \tag{20}$$

For the model in (1), $B(f)$ incorporates the characteristics of transmitter and receiver [22] so that $B(f)[dB] = 20log(B(f)) = TVR(f)[dB] + RVS(f)[dB]$. In order to study the channel characteristics excluding the effects of the transmitter and receiver, only de-embedded measurement data is used in the following analysis unless otherwise specified.

A. TRANSFER FUNCTIONS

We start with the measured basic path loss (19) as shown in Fig. 5 for 1 m ($z = 1$) separation between transducers. To understand the effects of the transmitter and receiver characteristics on the measurements, we also provide in Fig. 5 dashed lines denoting the reference channel $B(f)[dB] = TVR(f)[dB] + RVS(f)[dB]$. These were obtained for an air medium in an acoustic anechoic chamber while those for the water medium by the datasheet of the transducer. With respect to $B(f)[dB]$ it can be observed that signals in the pipes generally have less path loss, than in open air or water, and this is because the wave energy is confined to the pipe instead of radiating out. There are also differences between the air and water reference channel $B(f)[dB]$ and this is due to the specific transducer types (magnetic versus piezoelectric). As expected for this range of frequencies $B(f)[dB]$ has an f^4 dependence on frequency for the open water channel using piezoelectric transducers [22].

With the results in Fig. 5 we can obtain the de-embedded path loss as shown in Fig. 6. It can be observed that both

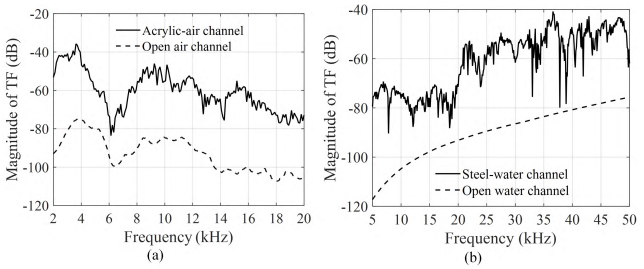

FIGURE 5. Magnitude of transfer functions (equivalent to path loss (19)) for the pipe channels and their respective calibration channels at 1 m seperations (a) acrylic-air channel, (b) steel-water channel.

sets of data have some similarity. Both sets have low loss at low frequencies which is followed by a path loss increase with frequency. Above a frequency of transition (6 kHz in air channel and 18 kHz in water channel), the path loss of both channels goes through abrupt amplitude changes. The variations in path loss as a function of frequency support the notion of destructive and constructive interference between multiple signal paths such as modes in this region. The abrupt amplitude increase at certain frequencies is evidence of the excitation of a new mode. An extract comparing two sets of results in which distance is doubled is also provided in Fig. 6 where it can be seen that the general structure of the transfer functions is maintained over this distance with a fairly constant attenuation across frequency. It can be deduced that path loss $e^{-\alpha z}$ only changes slowly with distance and this will be discussed in a later subsection.

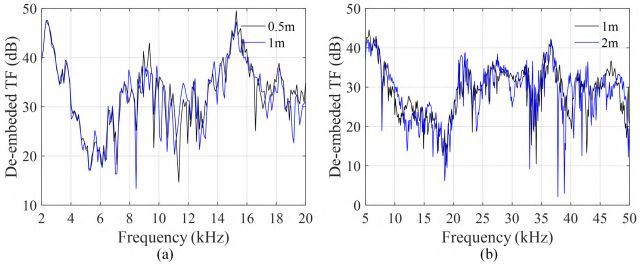

FIGURE 6. De-embedded transfer functions with respect to doubling of distance (a) acrylic-air channel, (b) steel-water channel.

B. DISPERSION CURVES

We next consider the measured $f - k_{nm}(f)$ dispersion curves. The spatial frequency response along equally separated distance z and wavenumber are Fourier transform pairs (3). Measured dispersion curves are plotted in Fig. 7 where model predictions have been added as dashed lines. From this set of rigorous measurements, we can extract the following channel information: (a) total number of modes with high energy (the threshold is 40 dB below the highest); (b) the frequency dependence of wavenumber of each mode, and consequently the relationship between phase velocity, group velocity and frequency; (c) the change of energy intensity of each mode with frequency; (d) the energy ratio between

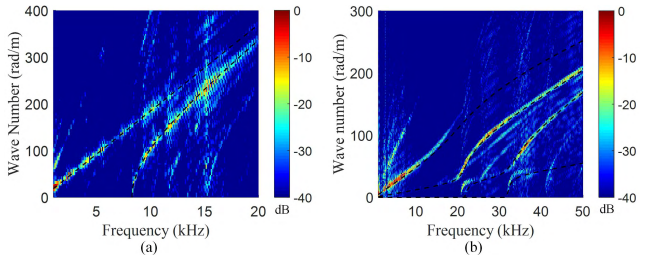

FIGURE 7. Measured $f - k_{nm}$ dispersion curves (a) acrylic-air channel, (b) steel-water channel. The overlaid dashed lines are for the predicted results as shown in Fig. 2.

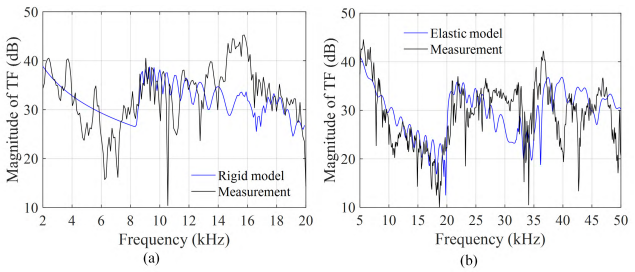

FIGURE 8. Comparison of modeled and measured transfer function (a) acrylic-air channel, (b) steel-water channel.

modes at each frequency. Comparisons with the model predictions show good agreement and those model predictions were extracted from the results in Fig 2. Due to the center positioning of the transducers we observe that modes with $n = 0$ are mainly observed.

In the acrylic-air channel, there exists four modes and the two main modes with significant energy include a plane wave mode (0,0) with zero cutoff frequency traveling at a constant speed of 340 m/s and a second mode (0,1) cut on at 8.2 kHz and its wave speed increases with the frequency increase and gradually converges to 340 m/s at high frequency. Energy intensity of both modes decreases with frequency increase. Two modes coexist from 8.2 kHz to 11.5 kHz. Below 8.2 kHz, the second mode has not been excited yet, while above 11.5 kHz, the energy of the first mode becomes negligible.

In the steel-water waveguide there exist seven modes. Below the first cutoff frequency at 20 kHz, mode (0,0) and mode (0,1) coexist, however the energy of mode (0,0) travels at around 1300 m/s and dominates in this frequency range. Mode (0,1) with extremely high wave speed (propagation in steel pipe wall) below 20 kHz starts to have significant energy between 20 kHz to 30 kHz where the wave speed drops to below wave speed in open water. After 32 kHz, mode (0,2) and mode (0,3) come in. Generally speaking, energy intensity of higher order modes are smaller than lower order modes, for example, mode (0,3) has very small energy. We also observe that when the signal group velocity is equal to or smaller than the wave speed in open water, the energy intensity of each mode and frequency are inversely correlated. There are two frequency zones where one mode has significantly higher energy than all the other modes including 5-18 kHz and 20-30 kHz. In those frequency zones, fading depth due to multi-mode effect is expected to be small. The deterministic delay spread, however, can still be large due to the wave dispersion within each mode. Fading and delay spread will be discussed in a later subsection.

The frequency response function (1) predicted by the model is compared with the measurement in Fig. 8. Note that the amplitude of each mode was obtained for the model from the measured dispersion curves as a function of frequency, due to the complexity of the actual acoustic transducer sources. With 3 circularly symmetric modes combined for acrylic-air channel and 4 circularly symmetric modes combined for steel-water channel, model and measurement agree in terms of the general trend of the transfer functions. Due to reflections in the pipes the predicted and measured transfer functions for this kind of comparison do not match perfectly but do follow the general trend.

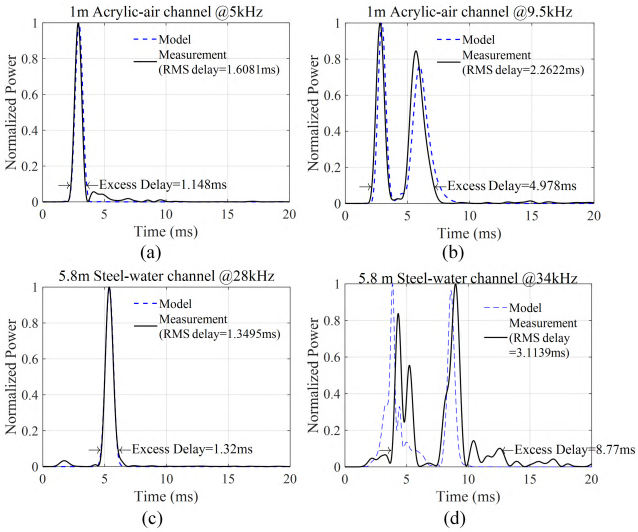

FIGURE 9. Various measured (solid lines) and predicted (dashed lines) normalized narrowband impulse responses.

C. NARROWBAND IMPULSE RESPONSES AND SPECTROGRAMS

By setting the window function in (10) to be a raised-cosine with $\Delta f = 1$ kHz and averaging over 20 measurement points ± 10 cm of the transducer position we can obtain the narrowband impulse responses of the channels (16). To provide some initial insight into these impulse responses we provide two results for the window centered at $f_0 = 5$ kHz and 9.5 kHz at $z = 1$ m in the acrylic-air pipe which are shown in Fig. 9. Similarly two results are also provided for the steel-water channel at $z = 5.8$ m this time at $f_0 = 28$ kHz and 34 kHz in the figure. The narrowband channel responses shown in Fig. 9 highlight the difference between a highly dispersive frequency band (longer RMS delay spread and excess delay) and weakly dispersive frequency band (shorter RMS delay spread and excess delay). The 4.5-5.5 kHz frequency band in

acrylic-air channel and the 27.5-28.5 kHz frequency band in steel-water channel are weakly dispersive, because most of the signal energy travels at the same wave speed in one mode and forms a main arrival path. The other arriving paths contain relatively low energy. However, the 9-10 kHz frequency band in acrylic-air channel and the 33.5-34.5 kHz frequency band in steel-water channel are highly dispersive bands, because of multimode propagation. Predicted narrowband responses using our model are also provided as dashed black lines and agreement can be observed.

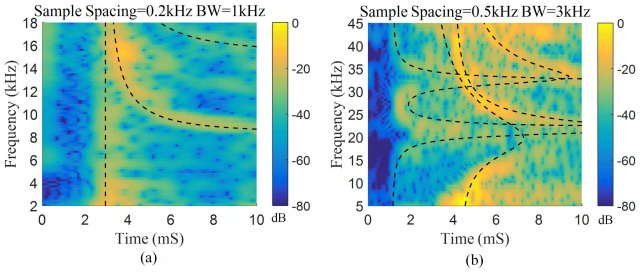

FIGURE 10. **Measured and predicted (dashed lines) channel spectrograms (a) acrylic-air channel @1 m, (b) steel-water channel @5.8 m.**

To illustrate all narrow band impulse responses across the entire frequency band we can use the spectrogram as defined in (11) where each frequency step index p or horizontal line represents the impulse response at one frequency. Spectrograms for both pipes are provided in Fig. 10. For the acrylic pipe $f_s = 2$ kHz, $p = [0, 80]$, $\Delta f = 1$ kHz and $\delta f = 0.2$ kHz respectively while for the steel pipe $f_s = 5$ kHz, $p = [0, 80]$, $\Delta f = 3$ kHz and $\delta f = 0.5$ kHz respectively for the spectrograms in Fig.10. Channel characteristics such as modes, cutoff frequencies, wavespeed and delay spread are easily observed in the spectrogram results. For convenience we have also plotted in these spectrograms black dashed lines which are the predicted spectrograms shown in Fig. 3 where close agreement can be observed. Due to the center positioning of the transducers we observe that modes with $n = 0$ are mainly observed.

In the acrylic-air channel, we again can observe that signals travel in modes. One mode identified as the vertical line at around 3 ms that exists across the entire band and has a constant group propagation speed of around 340 m/s (remember the spectrogram provides an indication of group velocity as shown in (5). Since the first mode has no dispersion (the $f - k_{mn}(f)$ relation is a straight line) group velocity and propagation speed of the air (340 m/s) are approximately the same as expected. It is also observed that two other modes are excited with cutoff frequencies at around 8 kHz and 15 kHz. These can be identified as the curves with a horizontal asymptotic at their cutoff frequency and the values agree well with the predicted spectrograms (3). This again demonstrates that modes in cutoff have large group delays and can even extend beyond our observation time of 10 ms. After cutoff it can also be observed that the group delay then reduces significantly and tends to that of the first mode.

In the steel-water channel, the spectrogram is more complicated than that of the acrylic-air channel but good agreement with our model as evidenced by the black dashed lines is also observed (also compare with (3)). As explained in the previous section, the elastic boundary condition leads to a more intricate relation between wavenumber and wave speed dispersion curve. Over the whole frequency range, there exist more than four modes, and two modes co-exist in the low frequency range. A distinctive phenomenon is that an early arriving signal path travels at a wave speed as high as 4800 m/s, which corresponds to the path arrival at around 1.2 ms and can be associated with a wave coupled into the steel pipe wall and traveling along the wall. The wave speed of the other modes are around or below 1480 m/s and are traveling in the water medium. The large difference in group velocities produces large delay spread of the channel in addition to the long delay spread due to wave dispersion.

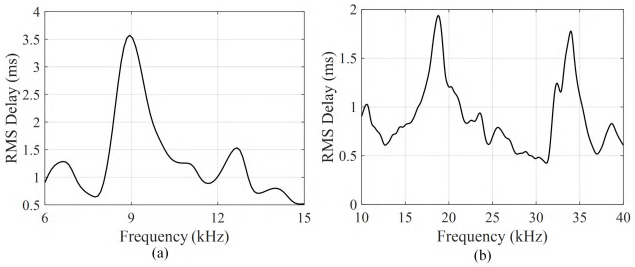

FIGURE 11. **Measured narrowband RMS delay spread as a function of frequency at 1 m separation (a) acrylic-air channel with $\Delta f = 1$ kHz, (b) steel-water with $\Delta f = 3$ kHz.**

From the narrowband model we can also estimate the delay spread (18) as a function of center frequency f_0 and these are shown in Fig. 11 for both channels. They show that the pipeline channels are frequency selective and delay spread becomes significantly larger at certain frequency bands (e.g. the neighborhood of 9 kHz in air channel and 20 kHz and 35 kHz in water channel). This again provides evidence that modes in cutoff are occurring at these frequencies. Modes in cutoff have low group velocity and therefore large delay spread. When comparing to the cutoff frequencies in Table 1 it can be observed that close agreement between the predicted modes and those observed experimentally are obtained. It should also be noted that since the transducers in both examples are located in the center of the pipeline we only expect to observe circularly symmetric modes such that $n = 0$. Therefore for the steel-water waveguide the cutoff frequencies of the observable modes are 0 kHz, 22.1 kHz and 32.1 kHz, while those for the acrylic-air waveguide are 0 kHz, 8.3 kHz and 15.2 kHz.

D. WIDEBAND IMPULSE RESPONSES

We can also characterize the acoustic pipeline in terms of wideband impulse response (13) and estimate wideband delay over the entire band for the acrylic and steel waveguide pipes (2-20 kHz and 5-50 kHz respectively). The measured

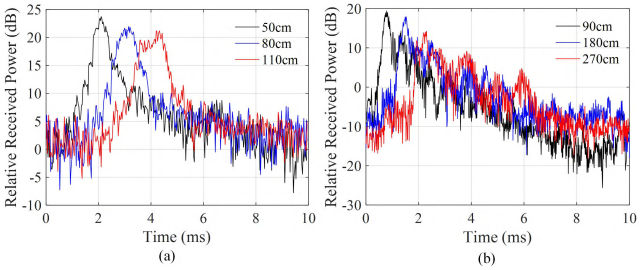

FIGURE 12. Measured wideband power delay profiles (a) acrylic-air channel, (b) steel-water channel.

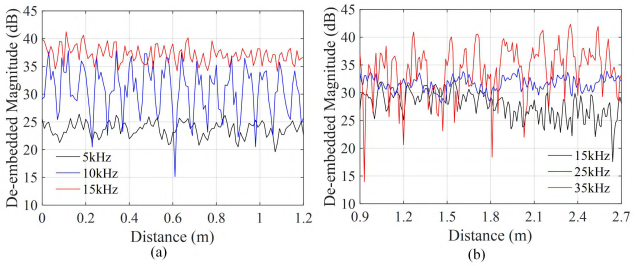

FIGURE 14. Measured channel fading as a function of distance (a) acrylic-air channel, (b) steel-water channel.

power delay profile (12) shows that an impulse signal is expanded to a more than 2.5 ms long pulse through the acoustic pipe channel. Most of the signal energy concentrates near several main paths, and signal energy decreases with time in general. It can be observed that the excess delay increases with distance. For acrylic air channel, the excess delay at 50 cm, 80 cm and 110 cm are 2.6 ms, 3.5 ms and 4.3 ms respectively. Similarly, the excess delay in steel water channel at 90 cm, 180 cm and 270 cm are 1.2 ms, 2.2 ms and 3.1 ms respectively.

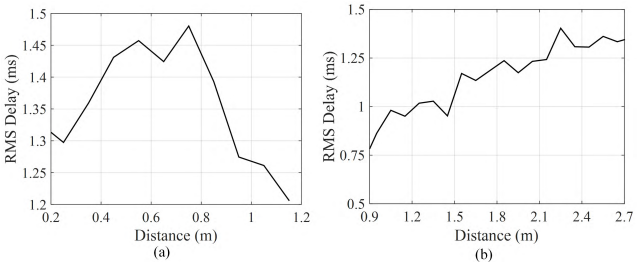

FIGURE 13. Measured wideband RMS delay spread as a function of distance (a) acrylic-air channel, (b) steel-water channel.

E. DISTANCE DEPENDENCE

It is also important to understand the distance dependence of the channel characteristics. A distinguishing property of the steel-water channel is that energy is confined inside the pipe. The path loss can be simplified as $e^{-\alpha(f)z}$ in (1) where $\alpha_{nm}(f)$ is the absorption coefficient of mode (n, m). The average path loss at different locations of the two pipes are measured and calculated by taking the mean value of path loss across the frequency band. As indicated earlier for Fig. 6 it can be observed that the attenuation is reasonably constant across the frequency bands. Steel water channel exhibits an average absorption coefficient of 0.98 dB/m, which is slightly smaller than 1.16 dB/m in acrylic-air channel. We have also examined the distance dependence on delay spread. Again we calculate the wideband RMS delay spread by (18) as shown in Fig. 13. In terms of RMS delay spread, in steel-water channel, the RMS delay spread generally follows an increasing trend as distance gets longer, and $\tau_{RMS}[ms] = 0.29z[m] + 0.61$. However, the RMS delay spread in the acrylic-air channel only increases with distance at first, then peaks at around 75 cm and then decreases with distance. A possible explanation of the difference in acrylic-air result is that signal paths with longer traveling time also endure higher attenuation, i.e. signals with longer delay disappear at longer distance.

F. FADING

Fading of the received signal as a function of distance z (or time t if the transducer is attached to a mobile robot) occurs because of the existence of multiple modes which can constructively and destructively interfere. If we consider two paths with amplitudes a_1 and a_2 and let $r_a = a_1/a_2$ the fading depth F_d is [26]

$$F_d = 20 * log(\frac{r_a^2 + 1 + 2r_a}{r_a^2 + 1 - 2r_a}). \tag{21}$$

In Fig. 14, received signal strength versus distance is plotted at three different frequencies for both pipe channels. The fading depths at signal frequency of 5 kHz, 10 kHz and 15 kHz are compared in acrylic-air channel and the fading depths at 15 kHz, 25 kHz and 35 kHz are compared in steel-water channel. The 10 kHz result in acrylic-air channel and the 35 kHz result in steel-water channel show more than 15 dB fading depth, which implies r_a is smaller than 2.45 and more than one signal path exists. Moreover, these two frequencies also fall into the long delay spread zone in Fig. 11. The other four results show less than 5 dB fading depth, which implies r_a is larger than 7.3. Hence, the energy of other signal paths are relatively small compared to the main path, and similarly these four frequencies fall into the short delay spread zone in Fig. 11. A conclusion is that significant fading occurs around cutoff frequencies and outside that range 1-2 paths mainly dominate the received signal and a small fading margin of 5dB would be appropriate. This is also backed up by the dispersion and spectrogram results where we generally see that only 1-2 paths dominate outside the cutoff zones.

G. NOISE POWER SPECTRAL DENSITY, LINK BUDGET AND CHANNEL CAPACITY

Noise power affects the signal to noise ratio (SNR) in acoustic communication, which directly determines the capacity of the channel formed by the transmitter and receiver pair. To complement our channel characterization we have therefore

obtained results for the noise power spectrum density (PSD) in the steel-water waveguide channel in order to estimate link budget and channel capacity. As a baseline reference it should be noted that noise in the ocean normally consists of background thermal noise and external environmental interference which dominates the thermal noise below 10 kHz and has been well documented [1]. At 10 Hz it has noise PSD of around 80 dB re μPa/$\sqrt{\text{Hz}}$ which decreases to around 20 dB re μPa/$\sqrt{\text{Hz}}$ at around 50 kHz (decay of 18 dB/decade [1]) and then starts to increase as thermal noise begins to dominate. To determine the noise PSD for our steel-water waveguide we use a low noise hydrophone (Teledyne Reson TC4032) which has an equivalent noise pressure around 20 dB below sea state zero and an RVS of -170 dB re μPa/V. This is connected to an NI USB-6356 multi-function data acquisition device which is configured into listening mode to record the acoustic noise in the water pipe. The noise signal in the steel-water waveguide in the laboratory was then acquired at 500 kSample/s at 16-bit resolution over a 48 hour period during a weekend when the lab was not in use. We found that the noise amplitude distribution was zero mean Gaussian and the estimated noise PSD in the water pipe was 70 dB re μPa/$\sqrt{Hz}$ at 10 Hz and decreased to 35 dB re μPa/$\sqrt{Hz}$ at 1 kHz providing an overall decay of 17 dB/decade. From 1 kHz to 50 kHz the noise PSD is approximately flat at 30 dB re μPa/$\sqrt{\text{Hz}}$ and it can be deduced that there are similarities to the noise PSD in the ocean.

With knowledge of the noise PSD it is possible to calculate link budget and therefore the possible range of communication in the pipes. The transmit voltage can be written as

$$V_{out}[\text{dBV}] = V_{in}[\text{dBV}] + TVR(f)[\text{dB}] - \alpha_{nm}(f)[\text{dB/m}] \cdot z - F_d[\text{dB}] + RVS(f)[\text{dB}], \quad (22)$$

where F_d is fading margin and taken here as 5 dB (see previous subsection) and the attenuation in dB is defined as $10\log(\exp(-\alpha_{nm}(f)))$=0.98 dB/m. The received noise voltage can also be be found as

$$V_{noise}[\text{dBV}] = V_{noise}^{pressure}[dB \text{ re } \mu Pa/\sqrt{\text{Hz}}] + 10\log(BW) + RVS(f)[\text{dB}], \quad (23)$$

where $V_{noise}^{pressure}[\text{dB re } \mu\text{Pa}/\sqrt{\text{Hz}}]$ is the noise PSD as described above and BW is the bandwidth in Hz. The ratio of the received power and noise PSD can then be used to determine SNR to give

$$SNR = V_{in}[\text{dBV}] + TVR(f)[\text{dB}] - \alpha_{nm}(f)[\text{dB}] \cdot z - F_d[\text{dB}] - V_{noise}^{pressure}[\text{dB re } \mu\text{Pa}/\sqrt{\text{Hz}}] - 10\log(BW). \quad (24)$$

As an example of a communication system consider operation in the 20-30 kHz acoustic band and requiring an SNR of at least 10 dB for successful reception. The noise can be considered to be Gaussian white noise at 30 dB re μPa/$\sqrt{\text{Hz}}$ level, and for a short time interval the channel can be assumed to be time-invariant. If the transmitter provides a peak output voltage of 10 V and taking TVR as 118 dB re μPa/V at 1 m then we can write the SNR as

$$SNR[\text{dB}] = 63[\text{dB}] - 0.98[\text{dB/m}]z. \quad (25)$$

Therefore for an SNR of 10 dB we can achieve a communication range of over 50 m demonstrating that acoustic communication in steel-water waveguides is indeed possible. It should also be noted that in our link budget we have used transducers that are primarily designed for use as hydrophones. If we used a transducer that was specifically tuned for transmission (projector) then it would be possible to achieve TVR's 10-20 dB higher providing an extra 10-20 m of range.

For the same 20-30 kHz frequency band, channel capacity can be obtained by the Shannon-Hartley theorem $C = BW log_2(1 + SNR)$ [28], [29]. The spectral efficiency ($\frac{C}{BW} = log_2(1 + SNR)$) under different input voltages and distances is plotted in Fig.15 where, again we take TVR as 118 dB re μPa/V at 1 m and the noise as 30 dB μPa/$\sqrt{Hz}$. We can observe that useful capacity can be obtained up to 50 m for V_{in} greater than 20 dBV.

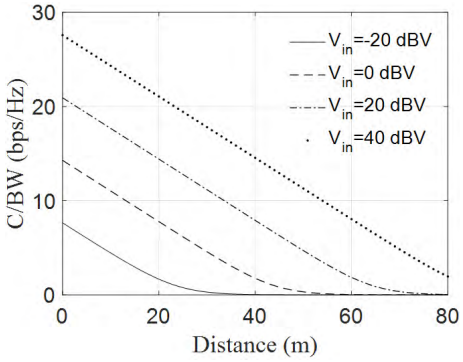

FIGURE 15. Bandwidth efficiency as a function of distance and transmitting voltage.

The final consideration is the delay spread. For the steel-water waveguide it is predicted there would be up to 5 modes and a delay spread of up to 15 ms (see section III.E), implying that equalization would be required to reach baud rates in excess of 50 symbols/second. Various equalization methods could be explored to increase the symbol rate significantly but this is beyond the scope of the current paper [30], [31], [32].

IV. CONCLUSION AND FUTURE WORK

A key contribution of this paper has been the reporting of experimental results and proposing a signal model for straight pipelines filled with gas or water. Comparisons of the model with measurements for both acrylic-air and steel-water acoustic waveguides show that the model accurately predicts essential channel features such as mode cutoffs, dispersion curves and delay spread. Other findings of the investigation are that propagation in rigid pipes is vastly different from that

in elastic pipes and that waveguides formed with water as the medium of propagation need to use an elastic pipe model even for seemingly rigid pipes such as steel. We also show that attenuation in both the waveguides, we considered, is around 1 dB/m and that delay spread depends on the dominating modes, the dispersion of each mode and the distance between transducers. It is also noted that at mode cutoffs the delay spread becomes very high and therefore communication, in bands that cover cutoff frequencies, needs to consider this effect. Noise PSD has also been measured, and combined with an estimate of the link budget, we determine that the range of communication in a steel-water pipe will be over 50 m. However, some form of equalization would be required if high data rates are to be obtained. We also show that channel spectrograms can be used as a straightforward method to determine dispersion characteristics.

Several important areas of future study are required. In order to extend this work to media which is flowing we need to move from static to dynamic conditions. The extension of the work to pipe networks consisting of several interconnected pipes and bent pipes is also required. Furthermore it would be useful to have channel characteristics over longer distances and for a larger variety of pipe materials and these issues will be considered in future work.

Appendix
FLEXIBLE BOUNDARY CONDITIONS AND CALCULATION OF WAVENUMBER

If the inner medium of the waveguide is liquid, acoustic waves propagate in both the inner liquid and pipe wall so that elastic boundary conditions must be utilized as follows

$$u_r^l\mid_{r=R_{in}} = u_r^s\mid_{r=R_{in}}, \tag{26}$$
$$p_r^l\mid_{r=R_{in}} = p_r^s\mid_{r=R_{in}}, \tag{27}$$
$$u_r^s\mid_{r=R_{out}} = 0, \tag{28}$$
$$p_r^s\mid_{r=R_{out}} = 0, \tag{29}$$

where the subscript l and s represent the inner liquid and the solid pipe wall media, $\mathbf{u} = (u_r, u_\theta, u_z)^T$ is velocity and p is pressure in which both quantities are matched across the solid pipe and the liquid at the inner pipe wall ($r = R_{in}$) and the outer pipe wall ($r = R_{out}$). These boundary conditions can be used to form characteristic equations to calculate the wavenumber k_{mn}. The matrix form of the characteristic equations is [19], [33]–[38]

$$\begin{bmatrix} L_{11} & L_{12} & L_{13} \\ L_{21} & L_{22} & L_{23} \\ L_{31} & L_{32} & L_{33} \end{bmatrix} \begin{bmatrix} u_r \\ u_\theta \\ u_z \end{bmatrix} = \begin{bmatrix} 0 \\ 0 \\ 0 \end{bmatrix}, \tag{30}$$

where

$$\begin{aligned} L_{11} &= -\Omega^2 + (k_{mn}R_{in})^2 + \frac{1}{2}(1-\nu)\, n^2, \\ L_{12} &= \frac{1}{2}(1+\nu)\, n\, (k_{mn}R_{in}), \\ L_{13} &= \nu\, (k_{mn}R_{in}), \\ L_{21} &= L_{12}, \\ L_{22} &= -\Omega^2 + \frac{1}{2}(1-\nu)\, (k_{mn}R_{in})^2 + n^2, \\ L_{23} &= n, \\ L_{31} &= L_{13}, \\ L_{32} &= L_{23}, \\ L_{33} &= -\Omega^2 + 1 + \beta^2 \left[(k_{mn}R_{in})^2 + n^2\right]^2 - FL, \end{aligned}$$

where $\Omega = 2\pi f R_{in}/c_s$, c_s is the wave speed of the pipe wall material, ν is the Poisson's ratio of the pipe wall material and $\beta = d/2\sqrt{3}R_{in}$ and is d is the pipe wall thickness. FL is the fluid load term given by

$$FL = \Omega^2\, (\rho_l/\rho_s)\, (h/R_{in}0)^{-1} \left(k_{mn}^r R_{in}\right)^{-1} \times [J_n\left(k_{mn}^r R_{in}\right)/J_n'\left(k_{mn}^r R_{in}\right)]$$

where $k_{mn}^r = \left(4\pi^2 f^2/c_l^2 - k_{mn}^2\right)^{1/2}$, c_l is the wave speed of the inner liquid, ρ is material density and $J_n(\cdot)$ and $J_n'(\cdot)$ are the the n^{th}order of Bessel function of the first kind and its derivative with respect to r. The k_{mn} that satisfies the boundary conditions required for is non-trivial solution of (30). Thus k_{mn} can be calculated by finding the root of the following equation

$$det\,(\mathbf{L}) = 0 \tag{31}$$

Due to the complexity of (31), k_{mn} is searched by root finding algorithms. The mode index m is then determined by the order of the the searched roots.

ACKNOWLEDGMENT

The authors are grateful for the help of the Department of Civil and Environmental Engineering at the Hong Kong University of Science and Technology for providing access and support for using their laboratories.

REFERENCES

[1] M. Stojanovic and J. Preisig, "Underwater acoustic communication channels: Propagation models and statistical characterization," *IEEE Commun. Mag.*, vol. 47, no. 1, pp. 84–89, Jan. 2009.
[2] M. Chitre, S. Shahabudeen, and M. Stojanovic, "Underwater acoustic communications and networking: Recent advances and future challenges," *Marine Technol. Soc. J.*, vol. 42, no. 1, pp. 103–116, 2008.
[3] T. S. Rappaport *et al.*, "Millimeter wave mobile communications for 5G cellular: It will work!" *IEEE Access*, vol. 1, pp. 335–349, May 2013.
[4] G. D. Durgin, T. S. Rappaport, and H. Xu, "Measurements and models for radio path loss and penetration loss in and around homes and trees at 5.85 GHz," *IEEE Trans. Commun.*, vol. 46, no. 11, pp. 1484–1496, Nov. 1998.
[5] D. Cassioli, M. Z. Win, and A. F. Molisch, "The ultra-wide bandwidth indoor channel: From statistical model to simulations," *IEEE J. Sel. Areas Commun.*, vol. 20, no. 6, pp. 1247–1257, Aug. 2002.
[6] M. D. Feit and J. A. Fleck, "Light propagation in graded-index optical fibers," *Appl. Opt.*, vol. 17, no. 24, pp. 3990–3998, 1978.
[7] R. B. Levin, P. R. Epstein, T. E. Ford, W. Harrington, E. Olson, and E. G. Reichard, "US drinking water challenges in the twenty-first century," *Environ. Health Perspect.*, vol. 110, p. 43, Feb. 2002.
[8] "China's thirst for water," Dow Water and Process Solutions Co., Edina, MN, USA, 2011.
[9] A. W. W. Association *et al.*, "Buried no longer: Confronting America's water infrastructure challenge," in *Proc. AWWA*, Denver, CO, USA, 2012, pp. 1–37.
[10] B. Mergelas and G. Henrich, "Leak locating method for precommissioned transmission pipelines: North American case studies," in *Proc. Leakage Conf.*, 2005, pp. 12–14.

[11] R. Fletcher and M. Chandrasekaran, "SmartBall: A new approach in pipeline leak detection," in *Proc. 7th Int. Pipeline Conf.*, 2008, pp. 117–133.
[12] B. Gulbahar and O. B. Akan, "A communication theoretical modeling and analysis of underwater magneto-inductive wireless channels," *IEEE Trans. Wireless Commun.*, vol. 11, no. 9, pp. 3326–3334, Sep. 2012.
[13] M. Chitre, "A high-frequency warm shallow water acoustic communications channel model and measurements," *J. Acoust. Soc. Amer.*, vol. 122, no. 5, pp. 2580–2586, 2007.
[14] M. C. Domingo, "Overview of channel models for underwater wireless communication networks," *Phys. Commun.*, vol. 1, no. 3, pp. 163–182, 2008.
[15] J. Catipovic, A. B. Baggeroer, K. von der Heydt, and D. Koelsch, "Design and performance analysis of a digital acoustic telemetry system for the short range underwater channel," *IEEE J. Ocean. Eng.*, vol. OE-9, no. 4, pp. 242–252, Oct. 1984.
[16] J. Armstrong, "OFDM for optical communications," *J. Lightw. Technol.*, vol. 27, no. 3, pp. 189–204, Feb. 1, 2009.
[17] S. Yarkan, S. Guzelgoz, H. Arslan, and R. R. Murphy, "Underground mine communications: A survey," *IEEE Commun. Surveys Tuts.*, vol. 11, no. 3, pp. 125–142, 3rd Quart., 2009.
[18] D. G. Dudley, M. Lienard, S. F. Mahmoud, and P. Degauque, "Wireless propagation in tunnels," *IEEE Antennas Propag. Mag.*, vol. 49, no. 2, pp. 11–26, Apr. 2007.
[19] C. R. Fuller, "The input mobility of an infinite circular cylindrical elastic shell filled with fluid," *J. Sound Vibrat.*, vol. 87, no. 3, pp. 409–427, 1983.
[20] G. Kokossalakis, "Acoustic data communication system for in-pipe wireless sensor networks," Ph.D. dissertation, Dept. Civil Environ. Eng., Massachusetts Inst. Technol., Cambridge, MA, USA, 2006.
[21] P. M. Morse and K. U. Ingard, *Theoretical Acoustics*. Princeton, NJ, USA: Princeton Univ. Press, 1968.
[22] J. L. Butler and C. H. Sherman, *Transducers and Arrays for Underwater Sound*. New York, NY, USA: Springer, 2007.
[23] J. Ma, M. J. S. Lowe, and F. Simonetti, "Measurement of the properties of fluids inside pipes using guided longitudinal waves," *IEEE Trans. Ultrason., Ferroelect., Freq. Control*, vol. 54, no. 3, pp. 647–658, Mar. 2007.
[24] A. L. Virovlyansky, A. Y. Kazarova, and L. Y. Lyubavin, "Ray-based description of normal modes in a deep ocean acoustic waveguide," *J. Acoust. Soc. Amer.*, vol. 125, no. 3, pp. 1362–1373, 2009.
[25] G. L. Turin, "Communication through noisy, random-multipath channels," Ph.D. dissertation, Massachusetts Inst. Technol., Cambridge, MA, USA, 1956.
[26] A. Goldsmith, *Wireless Communications*. Cambridge, U.K.: Cambridge Univ. Press, 2005.
[27] A. F. Molisch, *Wireless Communications*. New York, NY, USA: Wiley, 2012.
[28] M. Stojanovic, "On the relationship between capacity and distance in an underwater acoustic communication channel," *ACM SIGMOBILE Mobile Comput. Commun. Rev.*, vol. 11, no. 4, pp. 34–43, 2007.
[29] C. E. Shannon, "A mathematical theory of communication," *Bell Syst. Tech. J.*, vol. 27, no. 4, pp. 623–656, Oct. 1948.
[30] J. Zhang and Y. R. Zheng, "Frequency-domain turbo equalization with soft successive interference cancellation for single carrier MIMO underwater acoustic communications," *IEEE Trans. Wireless Commun.*, vol. 10, no. 9, pp. 2872–2882, Sep. 2011.
[31] M. Stojanovic, J. Catipovic, and J. G. Proakis, "Adaptive multichannel combining and equalization for underwater acoustic communications," *J. Acoust. Soc. Amer.*, vol. 94, no. 3, pp. 1621–1631, 1993.
[32] B. Li *et al.*, "MIMO-OFDM for high-rate underwater acoustic communications," *IEEE J. Ocean. Eng.*, vol. 34, no. 4, pp. 634–644, Oct. 2009.
[33] G. Pavić, "Vibrational energy flow in elastic circular cylindrical shells," *J. Sound Vibrat.*, vol. 142, no. 2, pp. 293–310, 1990.
[34] T. C. Lin and G. W. Morgan, "Wave propagation through fluid contained in a cylindrical, elastic shell," *J. Acoust. Soc. Amer.*, vol. 28, no. 6, pp. 1165–1176, 1956.
[35] D. H. Chambers, "Acoustically driven vibrations in cylindrical structures," Lawrence Livermore Nat. Lab., Livermore, CA, USA, Tech. Rep. LLNL-TR-645305, 2013.
[36] K. Baik, J. Jiang, and T. G. Leighton, "Acoustic attenuation, phase and group velocities in liquid-filled pipes: Theory, experiment, and examples of water and mercury," *J. Acoust. Soc. Amer.*, vol. 128, no. 5, pp. 2610–2624, 2010.
[37] J. Jiang, K. Baik, and T. G. Leighton, "Acoustic attenuation, phase and group velocities in liquid-filled pipes II: Simulation for spallation neutron sources and planetary exploration," *J. Acoust. Soc. Amer.*, vol. 130, no. 2, pp. 695–706, 2011.
[38] K. Baik, J. Jiang, and T. G. Leighton, "Acoustic attenuation, phase and group velocities in liquid-filled pipes III: Nonaxisymmetric propagation and circumferential modes in lossless conditions," *J. Acoust. Soc. Amer.*, vol. 133, no. 3, pp. 1225–1236, 2013.

LIWEN JING (S'15) received the bachelor's degree from the Harbin Institute of Technology, Harbin, China, in 2013, and the M.Phil. degree from The Hong Kong University of Science and Technology (HKUST), Hong Kong, in 2015. She is currently pursuing the Ph.D. degree with HKUST.

Her research interests include inverse problems in acoustic and electromagnetic waveguides with applications to defect detection in transmission lines and water pipelines; acoustic communication channel characterization and system design in fast fading channels including water pipelines; and RF and millimeter wave circuit and antenna design. She was a recipient of the Best Student Paper Award in 2016 MTT-S IWS Shanghai Conference.

ZHAO LI (S'13–M'17) received the B.Sc. and Ph.D. degrees in underwater acoustic engineering from Harbin Engineering University, Harbin, China, in 2010 and 2016, respectively. From 2014 to 2015, he was a Visiting Ph.D. Student with the University of Victoria. He is currently a Post-Doctoral Fellow with The Hong Kong University of Science and Technology.

His research interests include inverse problems in waveguide systems and ocean acoustics, Bayesian inference, acoustic signal processing, model-based Bayesian inversion, waveguide abnormality detection, and acoustic waveguide modeling. He was also involved in geo-acoustic inversion and navigation for underwater robots.

YUE LI (S'16) received the B.S. degree in information science and electronic engineering from Zhejiang University, Hangzhou, China, in 2015. He is currently pursuing the Ph.D. degree with the Department of Electronic and Computer Engineering, The Hong Kong University of Science and Technology, Hong Kong. His research interests include smart water systems, Internet-of-Things, and wireless communication.

ROSS D. MURCH (M'84–SM'98–F'09) received the bachelor's and Ph.D. degrees in electrical and electronic engineering from the University of Canterbury, New Zealand. He was the Department Head with HKUST from 2009 to 2015. His sabbatical in 2016 included visits to Imperial College London, MIT, and the University of Canterbury. He is currently a Chair Professor with the Department of Electronic and Computer Engineering, The Hong Kong University of Science and Technology (HKUST). His current research interests include the Internet-of-Things, underwater acoustics, and antenna design, and his unique expertise lies in his combination of knowledge from both wireless communication systems and electromagnetic areas. His research contributions include over 200 publications and 20 patents on wireless communication systems and antennas, and these have attracted over 12 000 citations. He received several awards, including the Computer Simulation Technology University Publication Award in 2015. He has served for IEEE in various positions, including area editor, technical program chair, distinguished lecturer, and the Fellow Evaluation Committee.